



HAL
open science

Long-term dynamics of Piton de la Fournaise volcano from 13 years of seismic velocity change measurements and GPS observations

Diane Rivet, Florent Brenguier, Daniel Clarke, Nikolai M. Shapiro, Aline Peltier

► To cite this version:

Diane Rivet, Florent Brenguier, Daniel Clarke, Nikolai M. Shapiro, Aline Peltier. Long-term dynamics of Piton de la Fournaise volcano from 13 years of seismic velocity change measurements and GPS observations. *Journal of Geophysical Research: Solid Earth*, 2014, 119, pp.7654-7666. 10.1002/2014JB011307 . insu-03581070

HAL Id: insu-03581070

<https://insu.hal.science/insu-03581070v1>

Submitted on 19 Feb 2022

HAL is a multi-disciplinary open access archive for the deposit and dissemination of scientific research documents, whether they are published or not. The documents may come from teaching and research institutions in France or abroad, or from public or private research centers.

L'archive ouverte pluridisciplinaire **HAL**, est destinée au dépôt et à la diffusion de documents scientifiques de niveau recherche, publiés ou non, émanant des établissements d'enseignement et de recherche français ou étrangers, des laboratoires publics ou privés.

Copyright

RESEARCH ARTICLE

10.1002/2014JB011307

Special Section:

Stress, Strain and Mass
Changes at Volcanoes

Key Points:

- We study the PdF volcano dynamics through seismic velocity changes from 2000 to 2013
- Long-term velocity decreases prior to the April 2007 eruption and increases afterward
- Seismic velocity changes and deformation have similar long-term trends

Correspondence to:

D. Rivet,
rivet@ipgp.fr

Citation:

Rivet, D., F. Brenguier, D. Clarke, N. M. Shapiro, and A. Peltier (2014), Long-term dynamics of Piton de la Fournaise volcano from 13 years of seismic velocity change measurements and GPS observations, *J. Geophys. Res. Solid Earth*, 119, 7654–7666, doi:10.1002/2014JB011307.

Received 21 MAY 2014

Accepted 4 SEP 2014

Accepted article online 8 SEP 2014

Published online 2 OCT 2014

Long-term dynamics of Piton de la Fournaise volcano from 13 years of seismic velocity change measurements and GPS observations

Diane Rivet¹, Florent Brenguier², Daniel Clarke¹, Nikolai M. Shapiro¹, and Aline Peltier¹

¹Institut de Physique du Globe de Paris, Sorbonne Paris Cité, CNRS (UMR7154), Paris, CEDEX 5, France, ²Institut des Sciences de la Terre, Université Joseph Fourier, Maison des Géosciences, Grenoble, France

Abstract We study the Piton de la Fournaise (PdF) volcano dynamics through the observation of continuous seismic velocity changes from 2000 to 2013. We compute the cross correlations of ambient seismic noise recorded at more than 30 short-period and broadband stations of the UnderVolc temporary seismic experiment and of the PdF volcano observatory network. The velocity changes are estimated from the travel time delay measured on the cross correlations computed between pairs of stations. We average the relative velocity changes for all pairs of stations and obtain a time series of the velocity change of Piton de la Fournaise volcano over 13 years. From the period 0.5 to 4 s, the depth sensitivity of the velocity change is ranging from approximately 100 m to 2500 m. A slow decrease of velocity is measured from 2000 and ends with a major eruption that occurred in April 2007. This eruptive episode is followed by an increase of the velocity. These long-term changes are compared to the deformation of the Piton de la Fournaise edifice estimated from geodetic measurements. An analysis of baseline change between GPS stations indicates an inflation of the volcanic edifice prior to April 2007 followed by a deflation since then. This deflation predominantly affects the terminal cone. Seismic velocity changes and deformation have similar long-term trends with velocity decrease observed during inflation and velocity increase during deflation. However, the velocity change magnitude is about 2 orders of magnitude greater than the deformation. This suggests nonlinear relation between velocity changes and deformation.

1. Introduction

Piton de la Fournaise (PdF) is a basaltic shield volcano located on the eastern side of La Réunion Island, in the Indian Ocean, 800 km east of Madagascar. La Réunion Island and especially the PdF volcano are the latest manifestation of the mantle plume that generated India's Deccan Traps during the Cretaceous [Duncan *et al.*, 1989]. PdF volcano is one of the most active volcanoes in the world with 58 eruptions since 1985 [Roult *et al.*, 2012; Peltier *et al.*, 2009a]. Its active caldera, inside which the current terminal cone is built, is 2600 m high and 10 km wide (Figure 1a). From a review of PdF volcano eruptions proposed by Vlastélic *et al.* [2009], the rate of magma production seems to have increased during the twentieth century and is particularly high since 1998. Eruptions are generally small effusive events that last a few days to a few months. However, much larger eruption can occur like the one that happened between 2 April and 1 May 2007, ejecting a volume of over $240 \times 10^6 \text{ m}^3$ of lava and during which the Dolomieu crater collapsed to form a new caldera at the summit [Michon *et al.*, 2007; Staudacher *et al.*, 2009]. Since that time, the volcanic activity decreased [Roult *et al.*, 2012].

Over the last decade, the increasing number of continuous seismometers and GPS operated by the Piton de la Fournaise observatory has improved the quality of the continuous monitoring of the volcano activity. Changes in the volcano activity produce changes in the mechanical properties of the medium that result in deformation and variations of the seismic wave velocity. Geodetic methods provide a measure of the displacements at the surface and are therefore strongly affected by local and shallow perturbations such as eruptions. Seismic wave velocity changes offer complementary information because seismic waves are sensitive to small perturbations of mechanical properties at depth within the volcano.

Measuring seismic velocity changes has been successfully applied in various areas of seismology and helped better constrain the dynamics of fast evolving geological objects such as active faults [Wegler and Sens-Schönfelder, 2007; Brenguier *et al.*, 2008b; Chen *et al.*, 2010; Hobiger *et al.*, 2012], subduction zones [Rivet *et al.*, 2011, 2014], volcanoes [Haney *et al.*, 2009; Duputel *et al.*, 2009; Mordret *et al.*, 2010; Brenguier *et al.*, 2008a, 2011; Sens-Schönfelder *et al.*, 2014], and landslides [Mainsant *et al.*, 2012]. Continuous monitoring of the

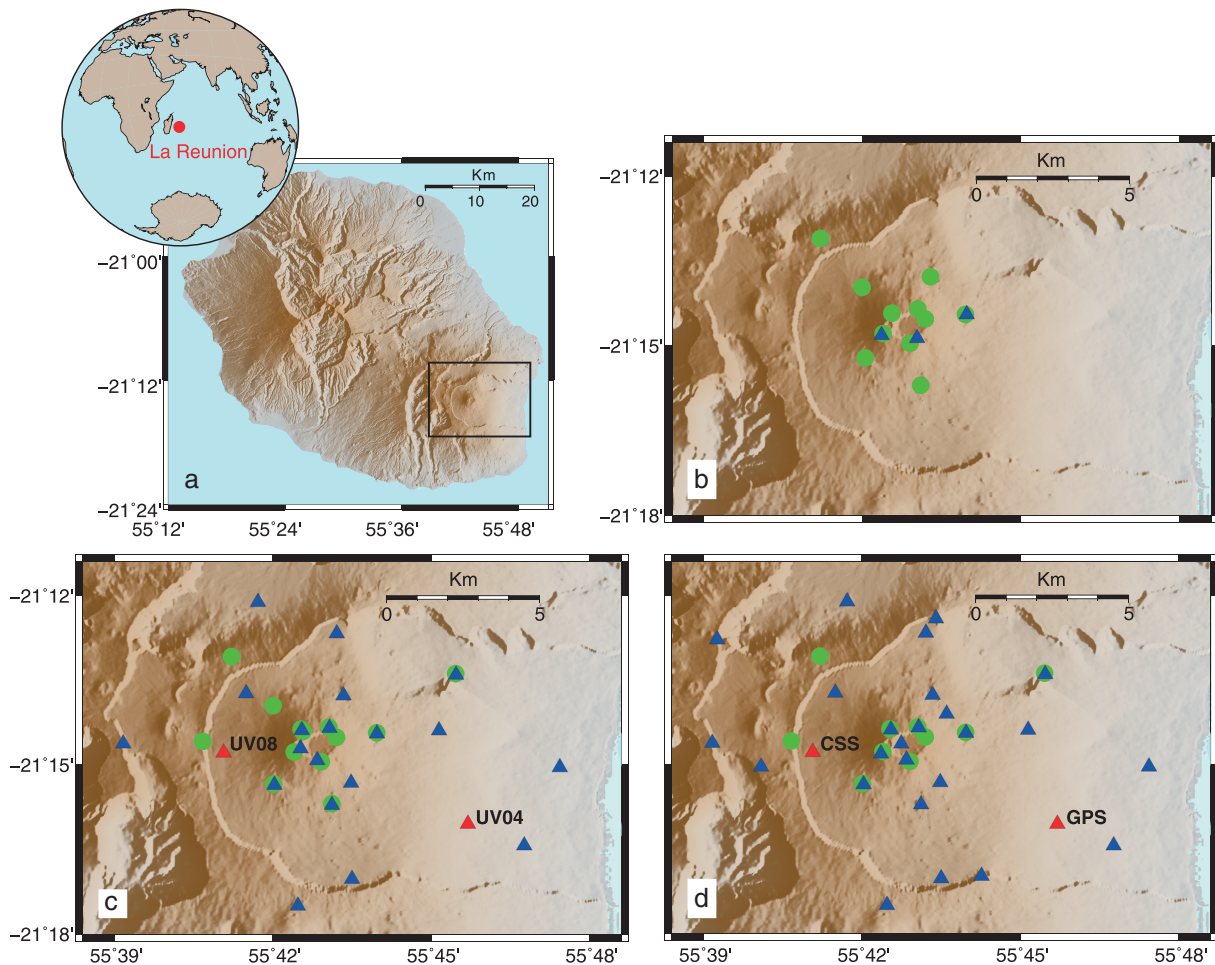


Figure 1. (a) Map of La Réunion Island with the location of the Piton de la Fournaise (PdF) volcano indicated by the square. Maps of the PdF seismic network (blue triangles) and GPS network (green circle) used to measure, respectively, seismic velocity changes and relative baseline change time series during the time periods (b) 1999–2009, (c) 2009–2011, and (d) 2011–2013. Red triangles indicate positions of UV04 and UV08 stations during UnderVolc experiment (Figure 1c) and positions of GPS and CSS stations after the experiment (Figure 1d). These stations are an example of stations used to merge the velocity change time series.

velocity is achieved through the use of seismic ambient noise. The impulsive responses of the media, the Green's functions, are recovered from the cross correlations of random seismic wavefields such as seismic noise [Shapiro and Campillo, 2004; Campillo, 2006]. From the monitoring of the reconstructed seismic wave travel times, we recover the relative seismic velocity changes in the area of interest [e.g., Clarke *et al.*, 2011].

In volcanic context, the time evolution of the seismic velocity changes is related to the eruptive dynamics of the volcano. Duputel *et al.* [2009] identified that velocity drops occurred during summit inflations, whereas velocity increased during deflations. These velocity variations are interpreted to be related to the preeruptive stress buildup within the reservoir that dilates the edifice and opens cracks. Continuous measurements of velocity changes are therefore generally used to retrieve information about the strain time evolution [e.g., Brenguier *et al.*, 2008a, 2011] and its spatial distribution [Obermann *et al.*, 2013; Sens-Schönfelder *et al.*, 2014]. However, other phenomena can affect seismic velocity such as seasonal variations of possibly air pressure or temperature and rainfalls producing short-term velocity changes that are sometimes of the same magnitude as perturbation produced by the volcano activity [Sens-Schönfelder and Wegler, 2006]. Also, volcanoes exhibit flank instabilities and can result in decreases of the seismic velocity [Clarke *et al.*, 2013].

Many of these studies mentioned above were performed on PdF volcano, making this volcano one of the most studied using seismic noise correlation monitoring. Brenguier *et al.* [2008a] analyzed 18 months (July 1999 to December 2000) of continuous seismic records from PdF volcano observatory. For the first time, the authors observed seismic velocity changes associated with volcanic activity, with velocity reductions of about

0.1% before eruptions, superimposed on long-term variations. Duputel *et al.* [2009] analyzed 13 months (May 2006 to June 2007) that cover 3 eruptions and compared seismic velocity changes to deformation recorded by GPS. Applying a regionalization, they found that the strongest velocity variations concentrated in the summit area of PdF. Brenguier *et al.* [2011] showed velocity decreases not associated with eruptions interpreted to be related to intrusion that does not evolve into eruptions. Clarke *et al.* [2013] provided a 10 year time series of seismic velocity changes that highlighted that the velocity change produced by the March–April 2007 eruption is about 6 times larger than for previous eruptions. Recently, Sens-Schönfelder *et al.* [2014] using 2 years of continuous records (2010 and 2011) observed a long-term velocity increase of about 0.25% per year. In addition to this long-term trend and preeruptive seismic velocity decreases, the authors observed short-term velocity increases during posteruptive periods of deflation associated with subsidence observed by GPS. In addition, during the period investigated, they did not observe a dependence of the velocity change on the location of the erupting fissures. The authors interpreted that seismic velocity changes would reflect the dynamics of a shallow magma reservoir rather than the effect of the eruption at the surface.

In this study we measure the seismic velocity changes in the Piton de la Fournaise volcano using cross correlations of ambient seismic noise recorded continuously between 2000 and 2013. Following the approach of Brenguier *et al.* [2008a] and Clarke *et al.* [2013], we extend the time series from 2010 to mid-2013, and using the dense UnderVolc network, we improve the time series from 2008 to 2010. With a time series of more than 13 years, we observe long-term variations characterized by small-rate seismic velocity changes that were not clearly observed and not discussed in previous works. We then compare these results with the edifice deformation measured with GPS. Dense continuous GPS monitoring started only in 2004. The comparison of seismic velocity variations with the edifice deformation during 9 years reveals the main trend of the evolution of the PdF volcanic system characterized by the long-term volcano inflation prior to the major 2007 eruption followed by the long-term deflation after 2008.

2. Seismic Data and Methods

2.1. Seismological Data

Because of the evolution of the network throughout the years, we separately processed the seismic velocity changes for three time periods. The first period covers 1999–2009, the second 2009–2011, and the third 2011–2013 (Figure 1). Between 1999 and 2009, a total of 13 stations of the seismic volcano monitoring network operated by the PdF volcano observatory were available. Eight stations were located outside the caldera rime. Among these stations, 4 were located more than 7 km away from the volcano summit and were therefore not considered. The 5 other stations were located on the summit and the cone of the PdF volcano; however, only 3 were continuously recording during the whole period. Because most of the stations later installed during the UnderVolc experiment are located within the caldera rime, the sensitivity to seismic velocity changes is maximum below the PdF summit, whereas for the Observatoire Volcanologique du Piton de la Fournaise (OVPF) network, the sensitivity is more spread out around the summit. Then keeping a similar sensitivity over the 13 years we analyzed, we consider only the 3 stations located on the volcanic summit and cone (Figure 1b). Starting in November 1999 and ending in October 2009, the first long-term time series was measured from cross correlations of ambient seismic noise recorded by these three short-period stations measuring the vertical component of the velocity.

After October 2009, we used continuous seismic records of seismometers provide by the UnderVolc temporary experiment during which a high-resolution seismic network has been deployed on the PdF [Brenguier *et al.*, 2012]. With this campaign, 15 broadband seismic stations were installed on the PdF volcano (Figure 1c) and operated continuously from September 2009 to June 2011. In addition to the UnderVolc network, we used data recorded by 4 permanent broadband stations installed and maintained by the PdF volcano observatory. After the end of the UnderVolc experiment, most of these sites were reequipped with permanent broadband seismometers.

For the period following the UnderVolc campaign until May 2013, we use 19 broadband and 8 short-period stations operated by the PdF volcano observatory (Figure 1d). The feasibility to measure seismic velocity change at periods between 1 and 10 s with short-period sensors has been demonstrated by Brenguier *et al.* [2008a]. Combining the results from different instrument types produces systematic bias in interstation cross correlations. However, this bias is constant over time and therefore does not affect the relative phase shifts that we measure on the noise cross correlations.

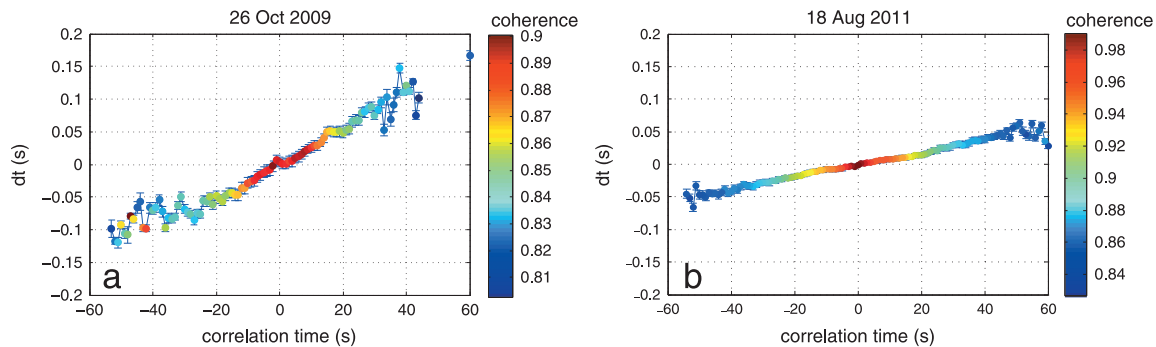


Figure 2. Distribution of the mean delay times measured for all pairs of stations (a) during and (b) after the UnderVolc experiment. Both mean delay times are computed relative to their reference correlation, which is the average of all correlations during the entire recording period. Colors indicate the mean coherence between current cross correlations and reference cross correlations, and error bars represent the mean error in the linear regression of the phase in the frequency domain to estimate delay times [Poupinet *et al.*, 1984].

2.2. Seismic Noise Processing and Cross Correlations

The procedure for seismic data processing and computing seismic noise cross correlations is described thereafter. After high-pass filtering at 0.1 Hz, we eliminate portions of signals with amplitude greater than 10 times the standard deviation calculated for the day. We then apply spectral whitening. From 1999 to 2009, the seismic ambient noise recorded at the three short-period stations is whitened in the frequency range of 0.1 to 1 Hz. During and after the UnderVolc experiment (2009–2013), ambient noise was whitened in a slightly higher frequency range of 0.25 to 2 Hz to be able to measure seismic velocity change that has a better sensitivity to shallow perturbations. Signals with amplitude greater than 3 times the standard deviation are then discarded. Finally, we applied a one-bit normalization on the whitened noise records.

Correlations between all pairs of stations are computed from consecutive records of seismic noise of 1 day length. These cross-correlation functions are calculated between vertical components retrieving mainly Rayleigh waves. To improve the signal-to-noise ratio in the correlations, we stack several days. The number of days we selected depends on the quality of noise records and the number of stations available in the network. For the period 1999–2009 for which only three stations are used, correlations are measured over a 30 day time window, while for the period 2009–2013, we used an 8 day time window.

2.3. Seismic Velocity Change Measurements

For the three time periods, i.e., 1999–2009, 2009–2011, and 2011–2013, and for each station pairs, we define reference cross correlation as the average of correlations during the entire time period. These references represent the average state of the surrounding medium where the seismic waves propagate. We estimate the seismic velocity change by measuring time delays between the current and the reference cross-correlation functions. If we assume a homogeneous seismic velocity change in the crust affecting the current cross-correlation, the relative difference in travel time gives the relative change in the seismic velocity: $dv/v = -dt/t$. We measure the travel time delays between -40 and 40 s of correlation time on direct and coda waves.

For any couple of reference cross correlation and current cross-correlation functions, the time delay between the two signals is measured using the multiple-window spectral analysis method originally proposed by Poupinet *et al.* [1984], also called Doublet method [e.g., Brenguier *et al.*, 2008a, 2008b]. The cross-correlations are divided into a series of short-time overlapping windows with central correlation time t . Within each window, apparent delay $dt(t)$ is measured from the phase shift measurements and a cross spectrum analysis of the two cross-correlation functions in the frequency domain. Seismic velocity change $dv/v = -dt/t$ is then determined using a linear regression of dt and t over all windows. Because we seek long-term variations characterized by small-rate velocity changes, we need to reduce as much as possible fluctuations in the seismic velocity change measure due to noise source variations for instance. A way of enhancing small but coherent small-rate velocity changes is to average the relative velocity changes over all station pairs available across the PdF volcano. Figure 2 gives examples of delay times measured during (Figure 2a) and after (Figure 2b) the UnderVolc campaign.

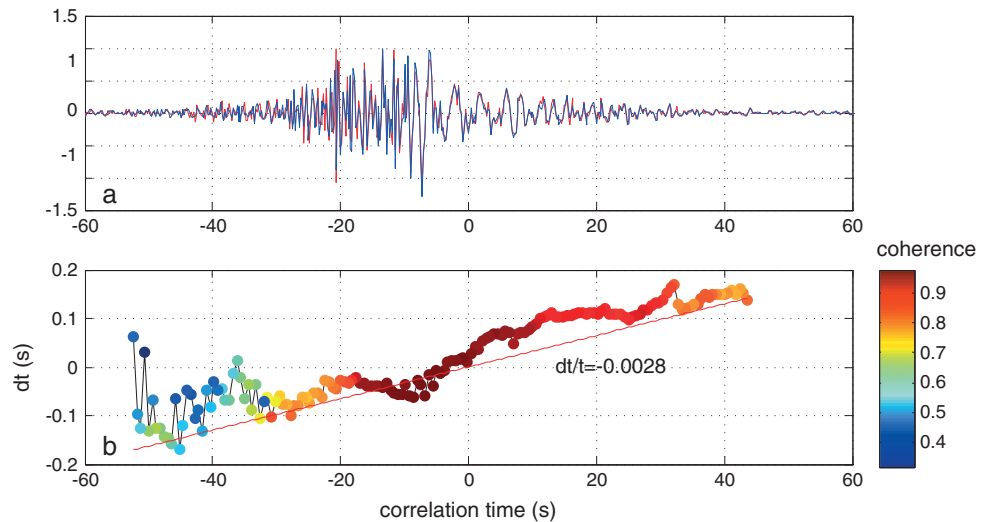


Figure 3. Travel time delay between the reference cross correlations computed during (UV04-UV08 station pair) and after (GPS-CSS station pair) the UnderVolc campaign. UV04 and UV08 stations have been replaced by GPS and CSS at the end of the campaign. Station locations are indicated by the red triangles in Figure 1. (a) Seismograms of the UV04-UV08 reference cross correlation (blue) and GPS-CSS reference cross correlation (red). (b) Distribution of delay times measured between the two reference cross correlations. Colors indicate the mean coherence between current cross correlations and reference cross correlations.

We obtain a velocity change time series for each time period, i.e., 1999–2009, 2009–2011, and 2011–2013. To merge the three time series, we compute the relative velocity changes between the reference cross-correlations of station pairs that stayed at the same sites for two successive periods. Figure 3 shows an example of travel time delay between the reference cross-correlations computed during (pair of stations named UV04 and UV08) and after (pair of stations named GPS and CSS) the UnderVolc experiment. Station locations are shown in Figure 1. UV04 and UV08 stations have been replaced by GPS and CSS exactly at the same sites at the end of the campaign.

3. Time Series of Seismic Velocity Changes From 2000 to 2013

We present the time series of seismic velocity changes from 2000 to 2013 (Figure 4a). The reliability of the velocity change measurements is estimated from both the coherency measured between the reference and the 30 day or 8 day cross-correlation functions and from the statistical error of the linear regressions of $dt(t)$ averaged for all the correlations according to Clarke *et al.* [2011] (Figure 4b). It can be seen that measurement errors became systematically smaller after 2009 when the number of stations used for measurements increased.

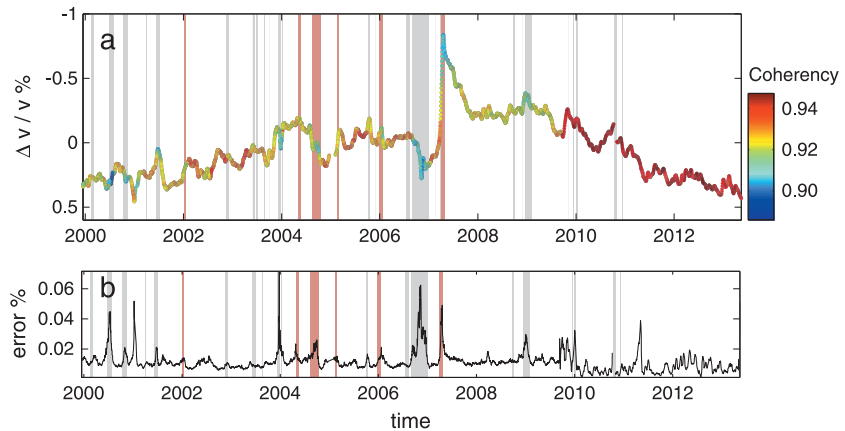


Figure 4. (a) Relative seismic velocity change time series from 2000 to May 2013 (velocity decrease is upward) and (b) error that represents the uncertainty of the linear slope estimation of dv/v . The gray bars mark the periods of eruptive activity. The red bars indicate major eruptions with a volume of ejected material greater than $15 \times 10^6 \text{ m}^3$.

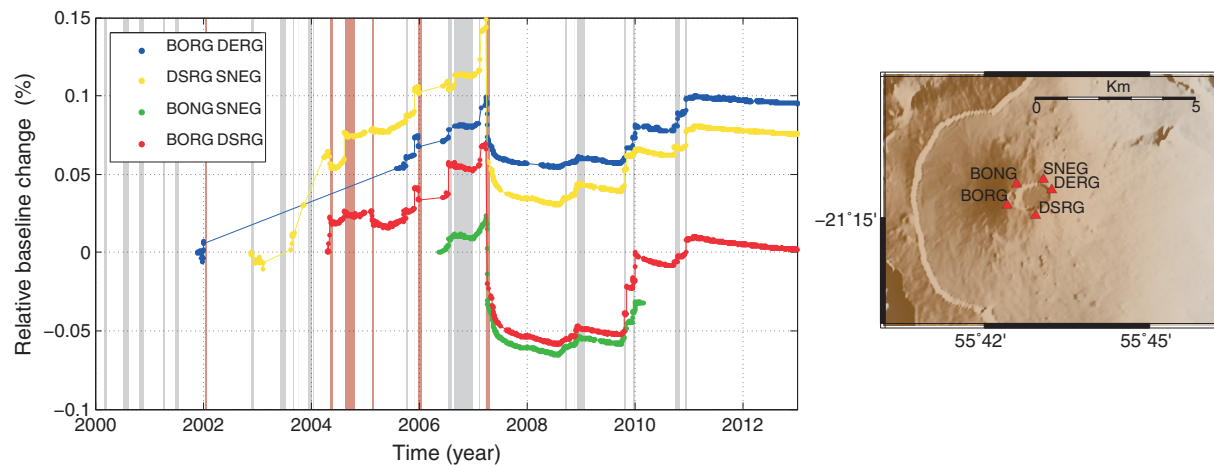


Figure 5. Daily relative baseline changes between GPS stations located around the summit crater as shown in the map.

Before the major eruption of March–April 2007, we observe a period of high volcanic activity with 31 eruptions that produced preeruptive short-term drops of the velocity of about 0.1% or less. These drops are generally followed by a recovery with an increase of the velocity. These variations are similar to the ones observed and described by *Brenguier et al.* [2008a] from July 1999 to December 2000. However, these variations are sometimes embedded in fluctuations of the seismic velocity. The most striking feature of the time series is a strong decrease in seismic velocity (-0.7%) that occurred in March–April 2007. In a finer analysis of the velocity change produced by the major eruption, *Clarke et al.* [2013] showed that the strong velocity decrease started on 30 March 2007 at the time of the dyke injection of the 30 March 2007 eruption and of the lateral magma injection toward the 2 April 2007 eruptive fissure. Then the velocity continued to decrease until 15 April with the slow movement of the eastern flank and the collapse of the summit crater on 5–7 April 2007. This large drop of velocity is followed by a recovery of the seismic velocity that lasted about 6 months. After this major volcanic event, the eruptive activity decreases with only 6 small eruptions since then. Besides the short-term seismic velocity changes related to eruptions, we observe a long-term evolution of the velocity. The first-order long-term velocity changes show that the seismic velocity decreases before the major eruption while it increases for the period following the eruption. Between 2000 and 2004, the velocity change decreased at a rate of $-0.1\% \text{ yr}^{-1}$. Then from 2004 to mid-2006, the velocity seems to decrease at a smaller rate. After the March–April 2007 eruption and the post-eruptive recovery that lasted until the end of 2007, the velocity remained constant for approximately 1.5 years, from early 2008 to mid-2009. Finally, after mid-2009, the velocity increased at a rate of $0.125\% \text{ yr}^{-1}$. The change of the long-term velocity trend after the March–April 2007 eruption suggests a modification of the regime of the PdF magmatic system with a reduction of the magmatic activity.

4. Deformation of the Piton de la Fournaise Volcano Using GPS Observations

Changes in the PdF dynamics produce seismic velocity variations and deformations of the volcanic edifice. This deformation can be detected by geodetic methods from space (interferometric synthetic aperture radar InSAR [e.g., *Massonnet et al.*, 1995; *Peltier et al.*, 2010a; *Clarke et al.*, 2013]) and in the field, with the use of tiltmeter, extensometer [*Peltier et al.*, 2005, 2006], and GPS [e.g., *Peltier et al.*, 2010b; *Sens-Schönfelder et al.*, 2014]). Here we use GPS baseline changes over time to estimate the long-term deformation of the Piton de la Fournaise volcano. GPS data have been processed with the GAMIT/GLOBK software package, which takes into consideration International GNSS Service (IGS) precise ephemeris, a stable support network of 20 IGS stations around La Réunion Island, a tested parameterization of the troposphere, and models of ocean loading, Earth, and Lunar tides.

Figure 5 shows relative baseline changes between GPS stations $\Delta l(t)/l(t_0)$ for the summit area from 2000 to 2013. The main feature of these time series is the brutal shortening of baseline distances associated to the March–April 2007 eruption and the Dolomieu crater collapse. *Staudacher et al.* [2009] and *Peltier et al.* [2009b] and *Staudacher and Peltier* [2014] described this feature. Before the March–April 2007 eruption, baseline

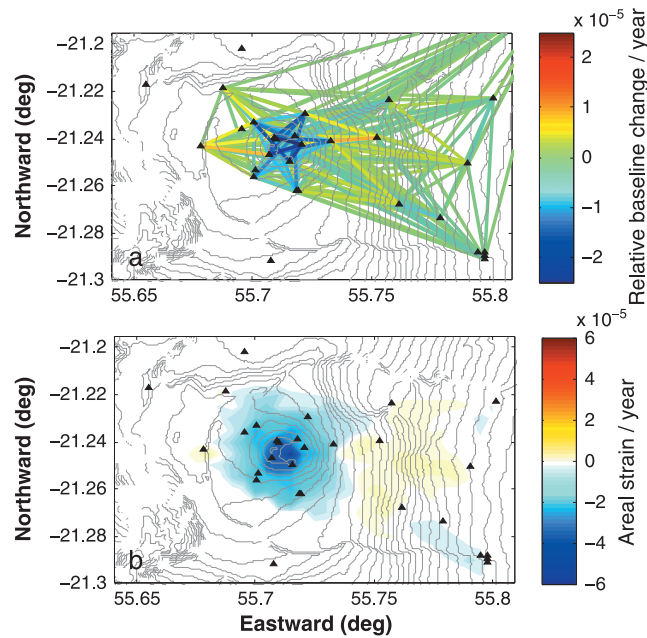


Figure 6. Tomography of the areal strain rate per year estimated during the interruptive period between March 2011 and March 2012. (a) Relative baseline change per year for all available GPS station pairs. (b) Regionalized areal strain rate per year. The negative values indicate the areas in deflation.

distances increased, indicating a long-term inflation of the volcano. This inflation was associated with numerous eruptions and intrusions and by continuous magma pressurization in depth [Peltier *et al.*, 2009b; Staudacher and Peltier, 2014]. After the March–April 2007 eruption, the baseline distances decreased for 15 months during the relaxation following the eruption and crater collapse [Peltier *et al.*, 2010b]. The deflation ended with the repressurization of the plumbing system and dyke intrusions preceding small successive summit eruptions (21 September to 2 October 2008, 27 November, and 14 December 2008 and 4 February 2009). However, from the long GPS time series presented in Figure 5, we observe that the deflation renewed after the recent eruptions. Since the March–April 2007 eruption, the PdF volcano is in deflation during all interruptive periods, suggesting a change in the volcanic regime [Peltier *et al.*, 2010b; Staudacher and Peltier,

2014]. In the following section, we focus on the interruptive deformation, first, its spatial extension and then its time evolution since 2004.

4.1. Tomography of the Interuptive Deformation After the March–April 2007 Eruption

From GPS baseline time series at the volcano summit (Figure 5), we observed that since the March–April 2007 major eruption, the interruptive periods are characterized by a deflation of the volcanic edifice. We analyze the spatial extension of the deflation from all GPS baselines available on the PdF from March 2011 to March 2012, which is the longest period without eruptions. Figure 6a shows the interruptive rates of the relative baseline changes for all available station pairs. The shortening of baseline distances is maximal for station pairs close to the volcanic cone.

To better estimate the spatial distribution of the deflation during the interruptive period, we regionalized the dilation per year. Assuming small deformation, the components of the strain tensor are defined as

$$\varepsilon_{ij} = \frac{1}{2} \left(\frac{\partial v_i}{\partial x_j} + \frac{\partial v_j}{\partial x_i} \right) \quad (1)$$

where i and j stand for east and north and v is the displacement.

The deformation produced by the volcano is expected to be dominated by the dilation. We thus assume the shear strain to be negligible in comparison to dilation. We expressed the areal strain as

$$\delta = \varepsilon_{ii} + \varepsilon_{jj} \quad (2)$$

Areal strain evolves in the same way as dilation because of the free surface. For instance, when dilation is in extension, areal strain is in extension too.

Besides, we assume the deformation to be isotropic; hence,

$$\varepsilon_{ii} = \varepsilon_{jj} = \varepsilon \quad (3)$$

We express $\varepsilon = du/dl$, du being the change of the unitary length dl . Thus, the areal strain is

$$\delta = 2\varepsilon = 2 \frac{du}{dl} \quad (4)$$

We identify the baseline changes for all available GPS pairs for March 2011 to March 2012. For a baseline p_i of length l_{p_i} between the GPS pair i , the relative baseline change can be expressed as

$$\frac{l_{p_i}(t_1) - l_{p_i}(t_0)}{l_{p_i}(t_0)} = \frac{\Delta l_{p_i}}{l_{p_i}(t_0)} \quad (5)$$

The change in the baseline length Δl_{p_i} is

$$\Delta l_{p_i} = \int_{p_i} du = \int_{p_i} \varepsilon dl = \int_{p_i} \frac{\delta}{2} dl \quad (6)$$

Thus, the relative baseline change is related to the areal strain through

$$\frac{\Delta l_{p_i}}{l_{p_i}(t_0)} = \frac{1}{2} \int_{p_i} \frac{dl}{l_{p_i}(t_0)} \delta \quad (7)$$

Equation (7) is similar to travel time integral along a ray on which many seismic tomographic methods are based. We therefore follow the approach of *Barmin et al.* [2001] that is based on ray theory with a Gaussian-shaped lateral smoothing. We invert the relative change rate in the baseline length between GPS receivers for the 2-D distribution of the isotropic areal strain rate in the medium. Because Δl_{p_i} is a linear function of δ , we define a model $m = \delta/\text{yr}$ and the observations $d = \frac{\Delta l_{p_i}}{l_{p_i}(t_0)}/\text{yr}$. Areal strain rate is discretized in a 22×35 Cartesian grid, where each cell of $520 \times 550\text{m}$ has a constant areal strain rate. With M being the number of cells in the model and N the number of baseline path, m is an M -long vector containing areal strain rate for every cell j , and d is an N -long vector with the relative baseline changes for every GPS pair i . We can write the forward problem in the following tensor notation.

$$d = Gm \quad (8)$$

with G as the forward operator representing the length of each baseline in each cell of the initial model divided by the initial baseline length. G is an $N \times M$ matrix that can be written as

$$G_{ij} = \frac{l_{ij}}{2 \times l_{p_i}(t_0)} \quad (9)$$

where l_{ij} is the length of the path i in the cell j . Using the *Barmin et al.*'s [2001] method, we estimate the areal strain rate by minimizing a penalty function composed of data misfit, model smoothness, and magnitude of perturbation, weighted by local path density.

Figure 6b presents the regionalization of the areal strain rate. The deflation concentrates at the volcanic edifice and tends to disappear away from the volcano. Another feature is the widespread slight areal strain rate of the eastern flank, which suggests that the large flank movement that initiates with the March–April 2007 eruption is still ongoing but with a much lower induced deformation $2 \times 10^{-5}/\text{yr}$ versus $10^{-4}/\text{yr}$ in 2007 [Clarke et al., 2013; Staudacher and Peltier, 2014].

Following *Barmin et al.* [2001] and *Mordret et al.* [2013], we assess the spatial resolution of the areal strain rate map using the resolution matrix at all cells (Figure 7). Figures 7a and 7b present the spike test resolution input and output, respectively, for a cell located at the volcano summit. Using the resolution matrices at every location, we fit a circle to the respective resolution map that encloses 50% of the recovered amplitude and takes its radius as estimation for the spatial resolution (Figure 7c). To estimate the lateral smearing of the inversion result, we also compute the distance between the center of the circle that fits the resolution map and the center of the input cell (Figure 7d). The spatial resolution shows that the region close to the PdF volcano summit and the eastern flank is well resolved with a resolution smaller than 2 km and with a resolution shift inferior to 1 km.

4.2. Average GPS Time Series From 2004 to 2013

We also process the GPS deformation time series to compare with seismic velocity changes. As shown in the previous section, relative baseline changes between GPS stations are related to the dilation of the volcano. To

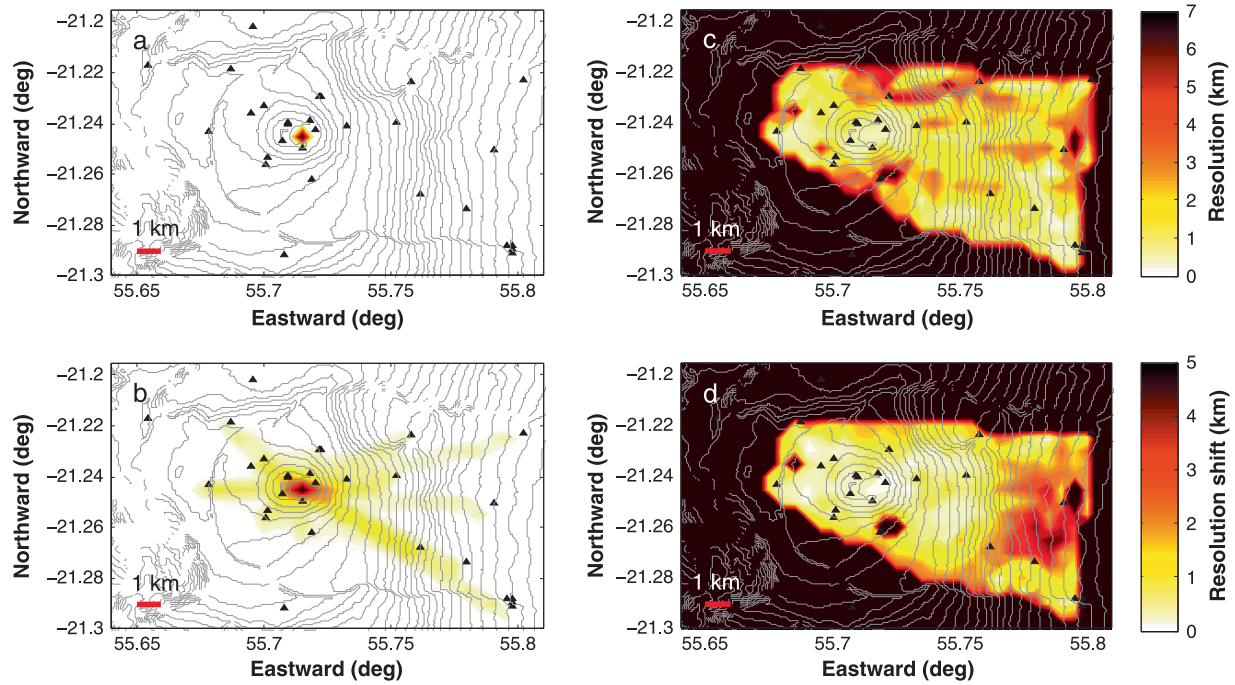


Figure 7. Spatial resolution of the inversion. Spike resolution at the PdF summit: (a) input and (b) output. (c) Spatial resolution map estimated from spike test analysis. Spatial resolution shift from the input location (Figure 7c). The black triangles indicate the GPS stations.

compute the average time series of the relative baseline changes, we consider GPS stations that are affected by the interruptive deformation around the terminal cone identified on the regionalization of the areal strain rate as shown in Figure 6b. The location of GPS stations is indicated in Figure 1. GPS is strongly sensitive to local static displacements produced by dyke intrusions during eruptions. These displacements result in sudden and permanent changes in the baseline time series. On the contrary, velocity changes have deeper sensitivity and are proxies of the average stress within the volcanic edifice [Sens-Schönfelder *et al.*, 2014]. Therefore, to compare deformation measured from GPS with seismic velocity changes, we need to minimize co-eruptive effects.

Volcanic eruptions and dyke intrusions produce large and sudden changes in the baselines that are very different from changes during intervolcanic periods characterized by slow deformations of small amplitude. Changes of the baseline p of length l_p have two contributions: the high-amplitude short-term co-eruptive and low-amplitude long-term interruptive displacements,

$$\Delta l_p(t) = \Delta l_p^{\text{eruptive}}(t) + \Delta l_p^{\text{interruptive}}(t). \quad (10)$$

In the following paragraph, we want to focus particularly on the long-term interruptive deformation susceptible to be related to the observed long-term seismic velocity changes. The time derivative of the baseline change for each interruptive period is close to constant:

$$\frac{\partial l_p^{\text{interruptive}}(t)}{\partial t} \approx \text{const}, \quad (11)$$

while during eruptions, the time derivative has large amplitude with

$$\frac{\partial l_p^{\text{eruptive}}(t)}{\partial t} \gg \frac{\partial l_p^{\text{interruptive}}(t)}{\partial t} \quad (12)$$

We minimize high-amplitude displacements produced by volcanic eruptions by an analysis of the time derivative of the baseline changes. We identify values in the derivative during eruptions that exceed 10 times the standard deviation. We replace these utmost values by the mean of the derivative estimated on 20 days before and 20 days after the eruption. We then obtain the interruptive baseline change by integrating the derivative after removing jumps caused by the eruptions. Figure 8 presents an example of baseline

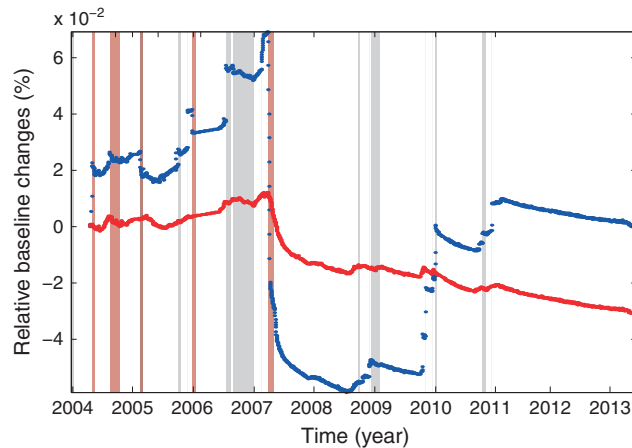


Figure 8. Relative baseline changes for GPS station pair BORG-DSRG (blue) and same after removing coeruptive displacements (red).

change time series before (blue) and after (red) removing coeruptive changes for the pair of GPS stations named BORG and DSRG. We apply the same strategy for all baselines. Finally, we measure the average intereruptive relative baseline changes considering all baselines located around the PdF edifice.

All the relative baseline change times series do not initiate at the same time. Different starting times of the time series produce steps when averaging the baselines for different pairs of GPS stations. To remove those steps, we proceed similarly as we did to minimize the coeruptive baseline changes. We replace the values of the derivative

that exceed 10 times the standard deviation by the mean of the derivative estimated on 20 days before and after the step.

5. Discussion and Conclusion

Figure 9 presents the comparison between the seismic velocity change time series (Figure 9a) and the mean relative baseline change on the PdF volcano (Figure 9b). Prior to the large March–April 2007 eruption, the intereruptive baseline change is characterized by an inflation of about $6 \times 10^{-3}\%/yr$. This major eruption, unlike the other eruptions that occurred during these 13 years, represents a drastic change in the intereruptive deformation dynamics. The period following the March–April 2007 eruption is in deflation except for periods before the eruptions of 2008, 2009, and 2010 characterized by small inflation that could correspond to a slow filling of the magma plumbing system or dyke intrusions.

For the period preceding the March–April 2007 eruption with decreasing velocity, we could distinguish two trends in the seismic velocity. First, the period before 2004 is characterized by decreasing velocity at a rate of $\sim -0.1\% yr^{-1}$. This long-term decrease of the velocity is accompanied by short-term variations associated with eruptions or magmatic intrusions. *Brenguier et al. [2012]* showed that some short-term velocity

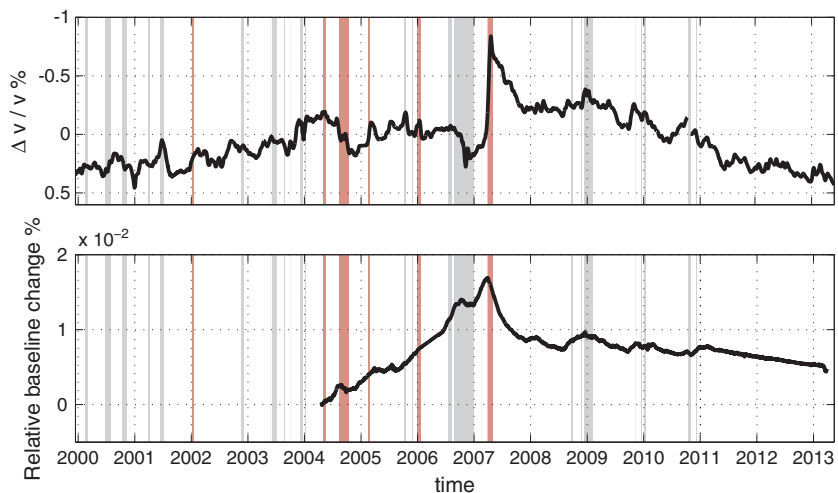


Figure 9. Comparison between seismic velocity changes and intereruptive relative baseline changes. (a) Seismic velocity change time series from 2000 to May 2013 (velocity decrease is upward). (b) Mean relative baseline change in percent for the intereruptive component of the deformation computed from all station pairs shown in Figure 8.

decreases that were not associated with eruption occurred during episodes of elevated seismicity. These velocity decreases were generally followed by an incomplete recovery of the velocity. The authors supposed different origins for those velocity decreases such as intrusions of magma not accompanied by eruptive activity or to pressure buildup associated with the replenishing of the magma reservoir. Second, from 2004 to 2007, the velocity seems to increase at a slower rate, while the dilation of the volcanic edifice was increasing. Possible explanations of this phenomenon are either that cracks reached the maximum opening or that the deep magma recharge terminated while the pressure increasing in the stored fluids produced dilation as seen by GPS as the surface. However, because transient velocity changes have large amplitude in comparison to the long-term variations, it is possible that the long-term velocity during the 2004–2007 continued decreasing at the same rate as before but was hidden by strong transients.

In March–April 2007, a large decrease of the velocity occurred. *Clarke et al.* [2013] demonstrated that the large movement of the eastern volcanic flank and volcanic edifice damaging resulted in this large velocity drop. This episode was followed by a post-eruptive recovery of the velocity until the end of 2008. After this recovery, the velocity change seems to remain steady for a year. Finally, the period following the beginning of 2009 is characterized by a long-term increase of the velocity that could be related to closing fissures and rock compaction in the volcanic edifice as suggested by the localization of the increasing velocity episode in 2010 and 2011 [*Sens-Schönfelder et al.*, 2014].

In addition to the seismic velocity change time series, we analyzed the temporal evolution of the inter-eruptive deformation of the PdF volcano from GPS measurements. A continuous inflation is observed prior to the March–April 2007 eruption followed by a deflation since then. The continuous summit inflation could be produced by different mechanisms such as magma crystallization, degassing of the magma stored in transitory reservoirs [*Tait et al.*, 1989], and a slow continuous filling [*Blake*, 1981]. These mechanisms could lead to decreasing velocity produced by tensile stress during enhanced pressurization in the volcanic edifice creating fissures and changes in the elastic properties. On the other hand, the deflation that concentrates around the PdF (Figure 6) could be a consequence of the destabilization due to the large withdrawal of the magma reservoir [*Peltier et al.*, 2010b]. Increasing velocity could be therefore related to closing fissures and rock compaction.

Long-term seismic velocity change observations are coherent with GPS measurements (Figure 9), with a decrease of seismic velocity prior to 2007 during inflation and followed by a decrease of the seismic velocity during deflation. However, for the period preceding the March–April 2007 eruption, from 2004 to 2007, increasing dilation is not associated with larger velocity decrease. A possible explanation could arise from the difference of depth sensitivity between velocity changes and GPS; the latter is strongly sensitive to shallow effects. Our observations confirm that at the time of the 2007 eruption, the PdF volcano was affected by a major change in the functioning of the magma feeding system leading to a change in its activity [*Peltier et al.*, 2010b; *Roult et al.*, 2012]. Contrary to the large March–April 2007 eruption, the numerous eruptions that occurred during the 13 year time series did not modify the long-term trends of increasing velocity.

Over the same period of time, seismic velocity variations are more than 1 order of magnitude stronger than strain (10^{-2} versus 10^{-4}) with a strain sensitivity of seismic velocity change on the order of 10^2 . *Egle and Bray* [1976] showed that anharmonic effects (third-order elastic constant) in rail steel could predict the measured velocity changes accurately. For the comparison in their experiments, the strain sensitivity of velocity change for shear and longitudinal waves was all below 3. As discussed by *Rivet et al.* [2011, 2014], the strong sensitivity of the seismic velocity to deformation cannot be explained by purely elastic anharmonic effects. Similarly, *Tsai* [2011] showed that the expected wave speed variations produced by hydrologic and/or thermoelastic variations using the elastic anharmonic effects account only for a small fraction of the observed seismic velocity seasonal changes. The strong strain sensitivity of seismic velocity changes implies important nonlinear behavior of the media. In laboratory experiments, deformation could result in strong seismic velocity decreases in rocks [e.g., *Johnson et al.*, 1996]. This is the so-called nonlinear elastic regime when strain affects the rock elastic modulus. The nonlinear effects are usually observed for a deformation greater than 10^{-6} and become more important with decreased effective pressure (increased pore pressure) in the media, which is likely the case for a volcanic edifice under pressure from the magmatic system.

This study presents continuous seismic velocity changes measured from 13 years of ambient noise records. Overall, we show that long-term small velocity changes can be accurately measured. Seismic velocity changes with their deeper sensitivity to changes in the elastic properties bring valuable, and complementary to geodetic observations, information about the long-term dynamics of the volcano over several years.

Acknowledgments

The data used for the analysis were collected by the Institut de Physique du Globe de Paris, Observatoire Volcanologique du Piton de la Fournaise (IPGP/OVPF). Another part of the data was collected by the Institut des Sciences de la Terre within the framework of ANR_08_RISK_011/UnderVolc project. For this project, we used seismic stations from the French mobile seismic network "Sismob" (INSU-CNRS). This work has been supported by ANR (France) under contract ANR-08-RISK-011 (UNDERVOLC) and by a FP7 European Research Council advanced grant 227507 (WHISPER) and by Emergences 2011 grant from the city of Paris. The data analysis was performed on the IPGP computer center S-CAPAD partially supported by Ile-De France via program SESAME and by CNRS via program MASTODONS.

References

- Barmin, M. P., M. H. Ritzwoller, and A. L. Levshin (2001), A fast and reliable method for surface wave tomography, *Pure Appl. Geophys.*, *158*, 1351–1375.
- Blake, S. (1981), Volcanism and the dynamics of open magma chambers, *Nature*, *289*(5800), 783–785, doi:10.1038/289783a0.
- Brenguier, F., N. M. Shapiro, M. Campillo, V. Ferrazzini, Z. Duputel, O. Coutant, and A. Nercessian (2008a), Towards forecasting volcanic eruptions using seismic noise, *Nat. Geosci.*, *1*(2), 126–130, doi:10.1038/ngeo104.
- Brenguier, F., M. Campillo, C. Hadziioannou, N. M. Shapiro, R. M. Nadeau, and E. Larose (2008b), Postseismic relaxation along the San Andreas fault at Parkfield from continuous seismological observations, *Science*, *321*(5895), 1478–1481, doi:10.1126/science.1160943.
- Brenguier, F., D. Clarke, Y. Aoki, N. M. Shapiro, M. Campillo, and V. Ferrazzini (2011), Monitoring volcanoes using seismic noise correlations, *C. R. Geosci.*, *343*(8–9), 633–638, doi:10.1016/j.crte.2010.12.010.
- Brenguier, F., et al. (2012), First results from the UnderVolc high resolution seismic and GPS network deployed on Piton de la Fournaise Volcano, *Seismol. Res. Lett.*, *83*(1), 97–102, doi:10.1785/gssrl.83.1.97.
- Campillo, M. (2006), Phase and correlation in 'random' seismic fields and the reconstruction of the Green function, *Pure Appl. Geophys.*, *163*(2–3), 475–502, doi:10.1007/s00024-005-0032-8.
- Chen, J. H., B. Froment, Q. Y. Liu, and M. Campillo (2010), Distribution of seismic wave speed changes associated with the 12 May 2008 Mw 7.9 Wenchuan earthquake, *Geophys. Res. Lett.*, *37*, L18302, doi:10.1029/2010GL044582.
- Clarke, D., L. Zaccarelli, N. M. Shapiro, and F. Brenguier (2011), Assessment of resolution and accuracy of the Moving Window Cross Spectral technique for monitoring crustal temporal variations using ambient seismic noise, *Geophys. J. Int.*, *186*(2), 867–882, doi:10.1111/j.1365-246X.2011.05074.x.
- Clarke, D., F. Brenguier, J.-L. Froger, N. M. Shapiro, A. Peltier, and T. Staudacher (2013), Timing of a large volcanic flank movement at Piton de la Fournaise Volcano using noise-based seismic monitoring and ground deformation measurements, *Geophys. J. Int.*, *195*(2), 1132–1140, doi:10.1093/gji/ggt276.
- Duncan, R. A., J. Backman, L. Peterson, and T. S. S. Party (1989), Reunion hotspot activity through tertiary time: Initial results from the ocean drilling program, leg 115, *J. Volcanol. Geotherm. Res.*, *36*(1), 193–198.
- Duputel, Z., V. Ferrazzini, F. Brenguier, N. Shapiro, M. Campillo, and A. Nercessian (2009), Real time monitoring of relative velocity changes using ambient seismic noise at the Piton de la Fournaise volcano (La Reunion) from January 2006 to June 2007, *J. Volcanol. Geotherm. Res.*, *184*, 164–173, doi:10.1016/j.jvolgeores.2008.11.024.
- Egle, D. M., and D. E. Bray (1976), Measurement of acoustoelastic and third-order elastic constant for rail steel, *J. Acoust. Soc. Am.*, *60*(3), 741–744.
- Haney, M. M., K. van Wijk, L. A. Preston, and D. F. Aldridge (2009), Observation and modeling of source effects in coda wave interferometry at Pavlof volcano, *Leading Edge*, *28*(5), 554–560, doi:10.1190/1.3124930.
- Hobiger, M., U. Wegler, K. Shiomi, and H. Nakahara (2012), Coseismic and postseismic elastic wave velocity variations caused by the 2008 Iwate-Miyagi Nairiku earthquake, Japan, *J. Geophys. Res.*, *117*, B09313, doi:10.1029/2012JB009402.
- Johnson, P. A., B. Zinszner, and P. N. J. Rasolofosaon (1996), Resonance and elastic nonlinear phenomena in rock, *J. Geophys. Res.*, *101*(B5), 11,553–11,564, doi:10.1029/96JB00647.
- Mainsant, G., E. Larose, C. Bronnimann, D. Jongmans, C. Michoud, and M. Jaboyedoff (2012), Ambient seismic noise monitoring of a clay landslide: Toward failure prediction, *J. Geophys. Res.*, *117*, F01030, doi:10.1029/2011JF002159.
- Massonnet, D., P. Briole, and A. Arnaud (1995), Deflation of Mount Etna monitored by spaceborne radar interferometry, *Nature*, *375*, 567–570.
- Michon, L., T. Staudacher, V. Ferrazzini, P. Bachèlery, and J. Marti (2007), April 2007 collapse of Piton de la Fournaise: A new example of caldera formation, *Geophys. Res. Lett.*, *34*, L21301, doi:10.1029/2007GL031248.
- Mordret, A., A. Jolly, Z. Duputel, and N. Fournier (2010), Monitoring of phreatic eruptions using Interferometry on Retrieved Cross-Correlation Function from Ambient Seismic Noise: Results from Mt. Ruapehu, New Zealand, *J. Volcanol. Geotherm. Res.*, *191*, 46–59, doi:10.1016/j.jvolgeores.2010.01.010.
- Mordret, A., M. Landès, N. M. Shapiro, S. Singh, P. Roux, and O. Barkved (2013), Studying seabed above the Valhall oil field with Ambient Noise Surface Wave Tomography, *Geophys. J. Int.*, *193*(3), 1627–1643, doi:10.1093/gji/ggt061.
- Obermann, A., T. Planès, E. Larose, and M. Campillo (2013), Imaging preruptive and coeruptive structural and mechanical changes of a volcano with ambient seismic noise, *J. Geophys. Res. Solid Earth*, *118*, 6285–6294, doi:10.1002/2013JB010399.
- Peltier, A., V. Ferrazzini, T. Staudacher, and P. Bachèlery (2005), Imaging the dynamics of dyke propagation prior to the 2000–2003 flank eruptions at Piton de La Fournaise, Reunion Island, *Geophys. Res. Lett.*, *32*, L22302, doi:10.1029/2005GL023720.
- Peltier, A., T. Staudacher, P. Catherine, L.-P. Ricard, P. Kowalski, and P. Bachèlery (2006), Subtle precursors of volcanic eruptions at Piton de la Fournaise detected by extensometers, *Geophys. Res. Lett.*, *33*, L06315, doi:10.1029/2005GL025495.
- Peltier, A., P. Bachèlery, and T. Staudacher (2009a), Magma transport and storage at Piton de La Fournaise (La Réunion) between 1972 and 2007: A review of geophysical and geochemical data, *J. Volcanol. Geotherm. Res.*, *184*(1), 93–108.
- Peltier, A., T. Staudacher, and P. Bachèlery (2009b), Formation of the April 2007 caldera collapse at Piton de La Fournaise volcano: Insights from GPS data, *J. Volcanol. Geotherm. Res.*, *184*(1–2), 152–163.
- Peltier, A., M. Bianchi, E. Kaminski, J.-C. Komorowski, A. Rucci, and T. Staudacher (2010a), PSInSAR as a new tool to monitor pre-eruptive volcano ground deformation: Validation using GPS measurements on Piton de la Fournaise, *Geophys. Res. Lett.*, *37*, L12301, doi:10.1029/2010GL043846.
- Peltier, A., T. Staudacher, and P. Bachèlery (2010b), New behaviour of the Piton de La Fournaise volcano feeding system (La Réunion Island) deduced from GPS data: Influence of the 2007 Dolomieu caldera collapse, *J. Volcanol. Geotherm. Res.*, *192*(1–2), 48–56, doi:10.1016/j.jvolgeores.2010.02.007.
- Poupinet, G., W. L. Ellsworth, and J. Frechet (1984), Monitoring velocity variations in the crust using earthquake doublets - An application to the Calaveras fault, California, *J. Geophys. Res.*, *89*(B7), 5719–5731, doi:10.1029/JB089B07p05719.
- Rivet, D., M. Campillo, N. M. Shapiro, V. Cruz-Atienza, M. Radiguet, N. Cotte, and V. Kostoglodov (2011), Seismic evidence of nonlinear crustal deformation during a large slow slip event in Mexico, *Geophys. Res. Lett.*, *38*, L08308, doi:10.1029/2011GL047151.

- Rivet, D., et al. (2014), Seismic velocity changes, strain rate and non-volcanic tremors during the 2009–2010 slow slip event in Guerrero, Mexico, *Geophys. J. Int.*, *196*(1), 447–460, doi:10.1093/gji/ggt374.
- Roult, G., A. Peltier, B. Taisne, T. Staudacher, V. Ferrazzini, and A. Di Muro (2012), A new comprehensive classification of the Piton de la Fournaise activity spanning the 1985–2010 period. Search and analysis of short-term precursors from a broad-band seismological station, *J. Volcanol. Geotherm. Res.*, *241*, 78–104, doi:10.1016/j.jvolgeores.2012.06.012.
- Sens-Schönfelder, C., and U. Wegler (2006), Passive image interferometry and seasonal variations of seismic velocities at Merapi Volcano, Indonesia, *Geophys. Res. Lett.*, *33*, L21302, doi:10.1029/2006GL027797.
- Sens-Schönfelder, C., E. Pomponi, and A. Peltier (2014), Dynamics of Piton de la Fournaise volcano observed by passive image interferometry with multiple references, *J. Volcanol. Geotherm. Res.*, *276*, 32–45, doi:10.1016/j.jvolgeores.2014.02.012.
- Shapiro, N. M., and M. Campillo (2004), Emergence of broadband Rayleigh waves from correlations of the ambient seismic noise, *Geophys. Res. Lett.*, *31*, L07614, doi:10.1029/2004GL019491.
- Staudacher, T., and A. Peltier (2014), *Ground Deformation at Piton de la Fournaise (La Reunion Island), A Review From 20 Years of GNSS Monitoring*, Springer Book, New York, in press.
- Staudacher, T., V. Ferrazzini, A. Peltier, P. Kowalski, P. Boissier, P. Catherine, F. Lauret, and F. Massin (2009), The April 2007 eruption and the Dolomieu crater collapse, two major events at Piton de la Fournaise (La Réunion Island, Indian Ocean), *J. Volcanol. Geotherm. Res.*, *184*(1–2), 126–137, doi:10.1016/j.jvolgeores.2008.11.005.
- Tait, S., C. Jaupart, and S. Vergnolle (1989), Pressure, gas content and eruption periodicity of a shallow, crystallising magma chamber, *Earth Planet. Sci. Lett.*, *92*(1), 107–123, doi:10.1016/0012-821X(89)90025-3.
- Tsai, V. C. (2011), A model for seasonal changes in GPS positions and seismic wave speeds due to thermoelastic and hydrologic variations, *J. Geophys. Res.*, *116*, B04404, doi:10.1029/2010JB008156.
- Vlastélic, I., C. Deniel, C. Bosq, P. Télouk, P. Boivin, P. Bachèlery, V. Famin, and T. Staudacher (2009), Pb isotope geochemistry of Piton de la Fournaise historical lavas, *J. Volcanol. Geotherm. Res.*, *184*(1), 63–78, doi:10.1016/j.jvolgeores.2008.08.008.
- Wegler, U., and C. Sens-Schönfelder (2007), Fault zone monitoring with passive image interferometry, *Geophys. J. Int.*, *168*(3), 1029–1033, doi:10.1111/j.1365-246X.2006.03284.x.